Solvent-Assisted Kinetic Trapping in Quaternary Perovskites

Darshan H. Parmar, Joao M. Pina, Hitarth Choubisa, Golam Bappi, Koen Bertens, and Edward H. Sargent*

Engineering halide perovskites through alloying allows synthesis of materials having tuned electronic and optical properties; however, synthesizing many of these alloys is hindered by the formation of demixed phases arising due to thermodynamically unstable crystal structures. Methods have been developed to make such alloys, such as solid-phase reactions, chemical vapor deposition, and mechanical grinding; but these are incompatible with low-temperature solution-processing and monolithic integration, precluding a number of important applications of these materials. Here, solvent-phase kinetic trapping (SPKT), an approach that enables the synthesis of novel thermodynamically unfavored perovskite alloys, is developed. SPKT is used to synthesize $Cs_{1-x}Rb_xPbCl_3$ and report the first instance of ultraviolet emission in polycrystalline perovskite thin films. SPKT leads to materials exhibiting superior thermal and photostability compared to non-kinetically trapped materials of the same precursors. Transient absorption spectroscopy of the kinetically trapped material reveals improved optical properties: greater absorption, and longer ground-state bleach lifetimes. SPKT may be applied to other perovskites to realize improved material properties while benefiting from facile solution-processing.

1. Introduction

Halide perovskites exhibit high photoluminescence (PL) quantum yields, defect tolerance, and straightforward processing.[1] The search for new bandgaps has led to studies of new alloys and dopants: for instance, Sn–Pb alloying reduces oxidation in Sn-based perovskites,[2] Pb-Mn alloying stabilizes the α-phase in iodide perovskites,[3] and Cs–Rb alloying widens the bandgap of perovskites into the ultraviolet (UV).[4] Incorporating alloys and dopants into the perovskite structure is complicated by the matter of phase stability. Synthetic methods that rely on solid-phase reactions, chemical vapor deposition, and mechanical grinding often diminish the benefits of facile low-temperature solution-processing.[4–6]

Here, we report perovskite alloys stabilized via solvent-phase kinetic trapping (SPKT). We highlight the approach by featuring $Cs_{1-x}Rb_xPbCl_3$ (CRPC), a perovskite alloy that is not readily synthesized using standard solution-processing. We synthesize CRPC from a hot precursor solution that is rapidly cooled and crystallized to obtain a kinetically trapped perovskite-phase CRPC thin film. The CRPC alloy constitutes the first report of UV emission from halide perovskite thin films.

2. Results and Discussion

The difficulty in forming certain perovskite alloys can be seen by examining the formation energy as a function of alloy composition (**Figure 1**a). The system is energetically driven to form the lowest energy phase, and this often is one of its non-alloy forms, making the formation of alloyed phases thermodynamically unlikely. In the case of Rb in CRPC, of interest in increasing the bandgap (Figure 1b) into the UV, the formation energy increases as the Rb content is increased (Figure 1a). As a result, Rb is expected not to incorporate, but instead to phase-segregate during synthesis. Details of these density functional theory (DFT) calculations can be found in the Supporting Information.

Alloys that are thermodynamically unstable at room temperature may form if their formation energy requirements are met. Hence, if the precursor solution is provided with sufficient thermal energy, it may be able to form the alloyed perovskite phase. However, this phase will be unstable; when slowly cooling to room temperature, the system will eventually revert to a non-alloy configuration as its formation energy requirements are no longer satisfied. To maintain a stable alloy, we thermally quench it as a final stage in synthesis, such that, from this elevated temperature, the alloyed phase cools rapidly to room temperature and avoids the crystal reorientation needed for phase segregation into non-alloyed domains.[7] This is our approach to achieve kinetic trapping. We use this strategy to develop alloys to tune perovskite bandgaps (Figure 1b) while preventing phase-segregation of Rb.

A schematic of the SPKT method is shown in **Figure 2**a. The precursors are initially dissolved in an organic solvent. The resultant solution is heated to a temperature of 150 °C while stirring; at this temperature, the alloy phase should be stable due to the negative Helmholtz free energy of mixing.[8] The heated solution is spin-coated onto a room-temperature glass substrate and room-temperature antisolvent is dropped

D. H. Parmar, J. M. Pina, H. Choubisa, Dr. G. Bappi, K. Bertens,
Prof. E. H. Sargent
The Edward S. Rogers Department of Electrical and Computer
Engineering
University of Toronto
27 King's College Circle, Toronto, Ontario M5S 3G4, Canada
E-mail: ted.sargent@utoronto.ca

The ORCID identification number(s) for the author(s) of this article
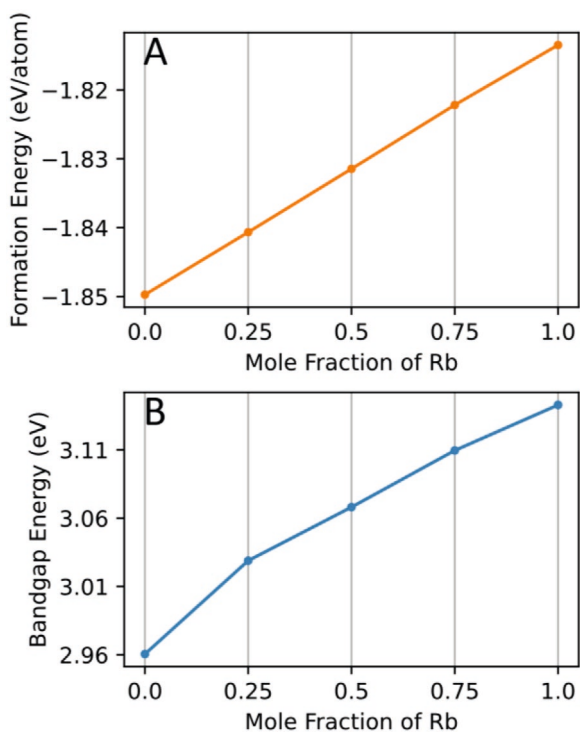can be found under https://doi.org/10.1002/adma.202008690.

**ADVANCED
SCIENCE NEWS**
www.advancedsciencenews.com

**ADVANCED
MATERIALS**
www.advmat.de

Figure 1. A) Formation energy, and B) bandgap energy of $Cs_{1-x}Rb_xPbCl_3$ as a function of x—the mole fraction of Rb as calculated with DFT.

to induce rapid crystallization. See Experimental Section for detailed procedure. Substitution of Cs^+ with Rb^+ in the $CsPbCl_3$ structure is known to cause octahedral tilting because of the smaller ionic radius of Rb^+; this ultimately leads to a wider

bandgap.[9,10] The incorporation of Rb^+ into $CsPbCl_3$ leads, for this reason, to a blueshift of the band edge. Therefore, we can gauge the degree of Rb incorporation by observing the absorption band edge of the material.

To test the SPKT method, we took aliquots of the precursor solution at different temperatures and spin-coated per Figure 2a, and we measured their absorption spectra. Figure 2b shows the Tauc plot of these absorption measurements, along with lines approximating the band edge. The inset plots the band edge energy in terms of wavelength with the aliquot temperature. From 20 to 80 °C there is a modest increase of 1.6 nm in the absorption band edge, due to slight increases in Rb-incorporation enabled by the higher temperature. From 80 to 130 °C, however, there is a dramatic increase of 9 nm in the absorption band edge. Further, when the temperature was increased to 110 °C, a secondary absorption feature appears. This suggests that the material reached a substitution limit whereby Rb could not be simply doped into $CsPbCl_3$, but instead there was sufficient energy to form a $Cs_{1-x}Rb_xPbCl_3$ alloy.[11] Thus, two separate phases are forming, one of Rb-doped $CsPbCl_3$ and another of alloyed $Cs_{1-x}Rb_xPbCl_3$.[11] We dub the former phase room-temperature (RT) and the latter alloyed-phase CRPC; subsequent analysis shows that there are substantial differences between these two materials. Due to multiple inflection points at these transition temperatures, a clear band edge could not be established for these aliquots. Thus, there is a transition between 110–120 °C, beyond which the solution has sufficient energy to form the CRPC phase. Adequately, from 130 to 160 °C there was again only one inflection point with a band edge close to 388 nm indicating a CRPC monophase. Thus, above the transition, we form a robust Cs–Rb perovskite alloy with a band edge in the UVA range. We opted to spin-coat our
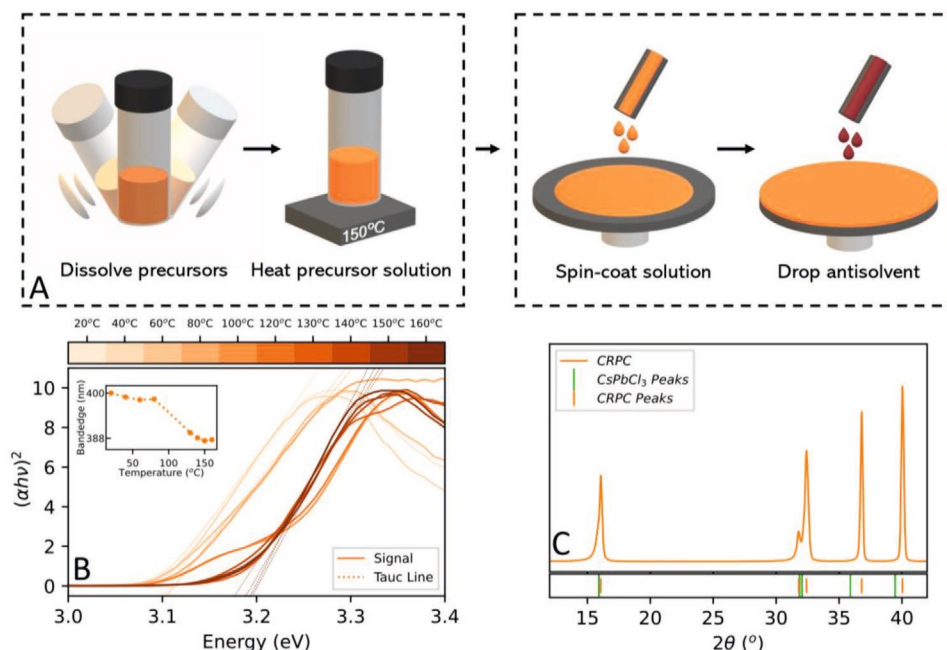

Figure 2. A) Schematic of solvent-phase kinetic trapping method. B) Tauc plot absorption spectra of $Cs_{1-x}Rb_xPbCl_3$ aliquots spin-coated at increasing temperatures. (Inset) Band edge wavelength at various temperatures. C) Powder X-ray diffractogram of CRPC (orange) along with corresponding peaks of $CsPbCl_3$ (green).
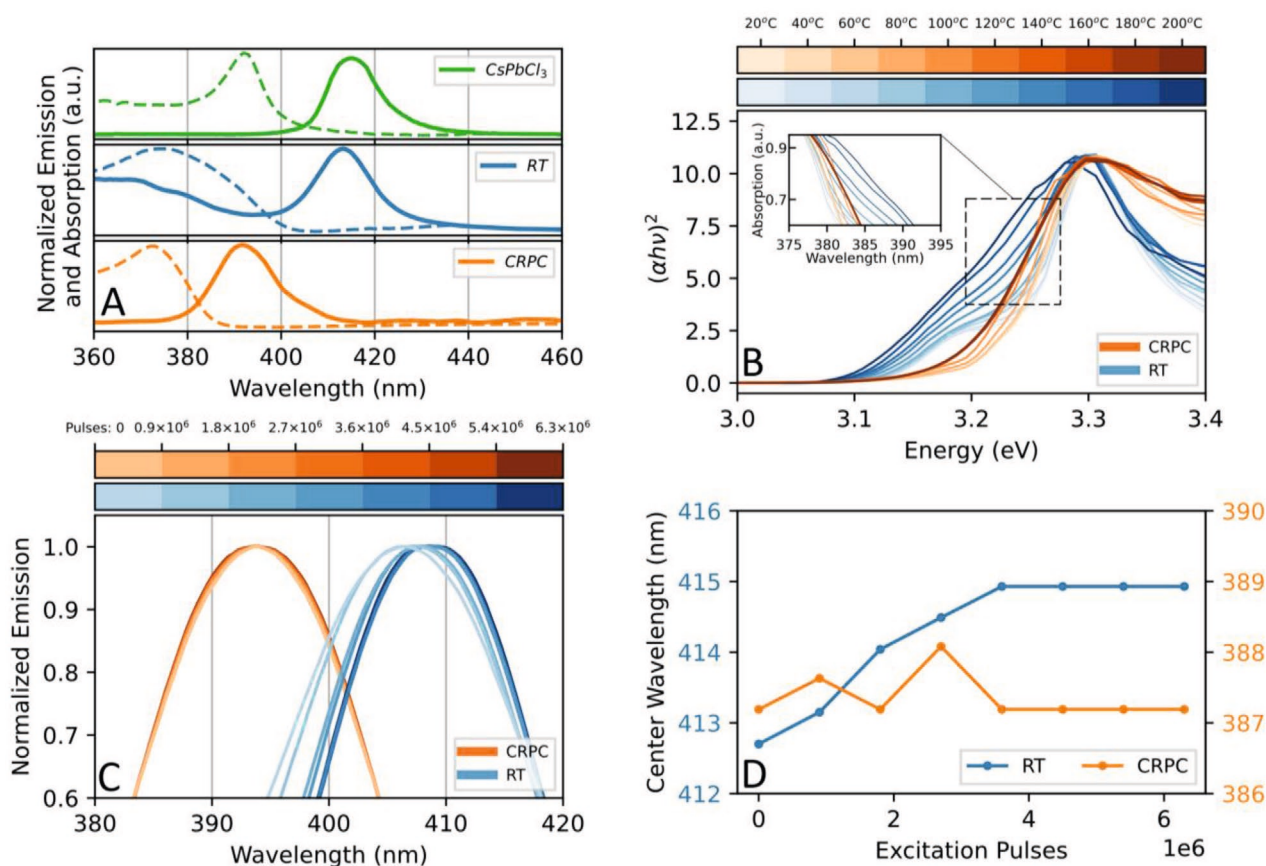
Figure 3. A) Absorption spectra (dashed lines) and emission spectra (solid lines) of CsPbCl$_3$ (green), RT (blue), and CRPC (orange). B) Absorption spectra as Tauc plots for CRPC (orange) and RT (blue) thin films at increasing temperatures. C) Emission spectra of CRPC (orange) and RT (blue) at increasing numbers of excitation pulses. D) Center wavelengths of emission from (C) plotted with corresponding number of excitation pulses.

samples at 150 °C to ensure there was sufficient thermal energy to facilitate a CRPC monophase.

Powder X-ray diffraction (PXRD) measurements allowed us to investigate changes in the unit cell upon Rb incorporation. Since Rb$^+$ has a smaller ionic radius than Cs$^+$, substitution is expected to lead to a smaller unit cell, as well as movement towards a monoclinic structure due to octahedral tilting.[4,12] This will shift PXRD peaks toward higher angles. CRPC peaks (orange) in Figure 2c are at higher angles than their corresponding CsPbCl$_3$ peaks (green). These shifts are comparable to lattice changes predicted using computational studies (See Figure S3, Supporting Information).

Photoluminescence and stability measurements were made to elucidate the merits of SPKT over room-temperature alloying (**Figure 3**). Figure 3a compares the emission and absorption spectra of CRPC thin films with CsPbCl$_3$ and samples spin-coated at room temperature. Absorption from CRPC thin films (Figure 3a orange dashed line) has a blueshift compared to pure CsPbCl$_3$ (green dashed line). The emission peak correspondingly shifts going from 415 nm (CsPbCl$_3$) to 392 nm (CRPC). This agrees well with the DFT studies of Figure 1b that predict a ≈15 nm blueshift with 50% Rb-incorporation.

We witnessed substantial differences between RT and CRPC. Here we prepared RT samples by spin-coating the precursor at room-temperature, instead of the 150 °C used for test samples.

In the RT samples, we did not see the blueshifts in the emission (Figure 3a blue solid line) spectra relative to CsPbCl$_3$. This complements the absorption observations of Figure 2b, suggesting that room temperature is insufficient to enable thorough Rb-incorporation.

Another issue with spin-coating at room temperature is the unreliability of the process. Despite well-controlled concentrations and spin-coating parameters, two distinct types of absorption spectra were observed, one with a single band edge and another with two absorption features (Figure S4, Supporting Information). This suggests that in the latter case, some CRPC domains are forming alongside domains of CsPbCl$_3$ with minute Rb doping.

For temperature-dependent absorption, we subjected as-prepared RT and CRPC thin film samples to increasing temperatures and measured their absorption spectra. The Tauc plots from this study are presented in Figure 3b. There is a gradual reduction in the band edge energy of CRPC with increasing temperature due to lattice expansion causing a decrease in bandgap in moderate temperature regimes (>100 K).[13,14] RT suffers a more dramatic redshift in the band edge; the inset shows this pronounced redshift more clearly. The RT samples used here have two absorption inflection points, suggesting they contain both CRPC domains and CsPbCl$_3$ domains with minute Rb-doping. Increasing temperature drives Rb out of

ADVANCED
SCIENCE NEWS
www.advancedsciencenews.com

ADVANCED
MATERIALS
www.advmat.de

the CRPC domains forming non-emissive phases, simultaneously this allows $CsPbCl_3$ to dominate the absorption spectra producing a dramatic redshift.[4] This demonstrates that room-temperature alloying produces an unstable material that suffers phase segregation at higher temperatures, while kinetic trapping produces an alloy that does not phase segregate.

To further challenge materials stability, we measured emission from CRPC and RT over 6×10^6 photoexcitation pulses (Figure 3c). A femtosecond laser at 330 nm and 5 kHz repetition was used to excite the samples with fluence of 0.375 µJ cm^{-2}. Figure 3d plots the center wavelength of the emission peaks, showing a clear upward trend in the emission wavelength of RT. There is a monotonic redshift of almost 2.5 nm over the excitation duration for the RT sample, while CRPC has only random fluctuations of less than 1 nm. The redshift in RT indicates segregation into a Rb-incorporated domain and a pure $CsPbCl_3$ domain.[11] From Figure 3a, there is only a minor blueshift between RT and $CsPbCl_3$; however, Figure 3d shows that this blueshift is entirely eliminated upon extended excitation. Eventually, the emission from RT becomes indistinguishable from $CsPbCl_3$ emission. Perovskites with lower ion migration activation energies suffer phase segregation

upon prolonged photoexcitation.[15] Thus, in RT, rubidium ions seem to be expelled to form pure $CsPbCl_3$ domains, and these domains ultimately become the dominant emitters.[11] Contrastingly, CRPC appears to retain its Rb-Cs alloying over prolonged photoexcitation as it does not experience a redshift. Thus, these results suggest that SPKT produces a more stable alloy by trapping the material in a metastable state.

Transient absorption spectroscopy (TA) measurements were also conducted; results are illustrated in **Figure 4**. The ground-state bleaches for all three materials are observed in Figure 4a.[16] Positive peaks attributed to photoinduced absorption are also evident.[17] $CsPbCl_3$ and CRPC samples exhibit very strong ground-state bleaches reaching less than −3 mOD at zero delay time, while the RT has a comparatively weaker bleach of ≈1.2 mOD. A weaker bleach peak suggests the RT has fewer active charge carriers, which can be attributed to a larger trap density in RT.[18]

This claim is further supported by the faster decay of the RT bleach relative to CRPC in Figure 4b. Because of their large bandgaps, inherent defects such as chloride vacancies produce deeper traps in CRPC and RT.[19] Thus, CRPC and RT have rapidly decaying ground-state bleaches compared to $CsPbCl_3$.
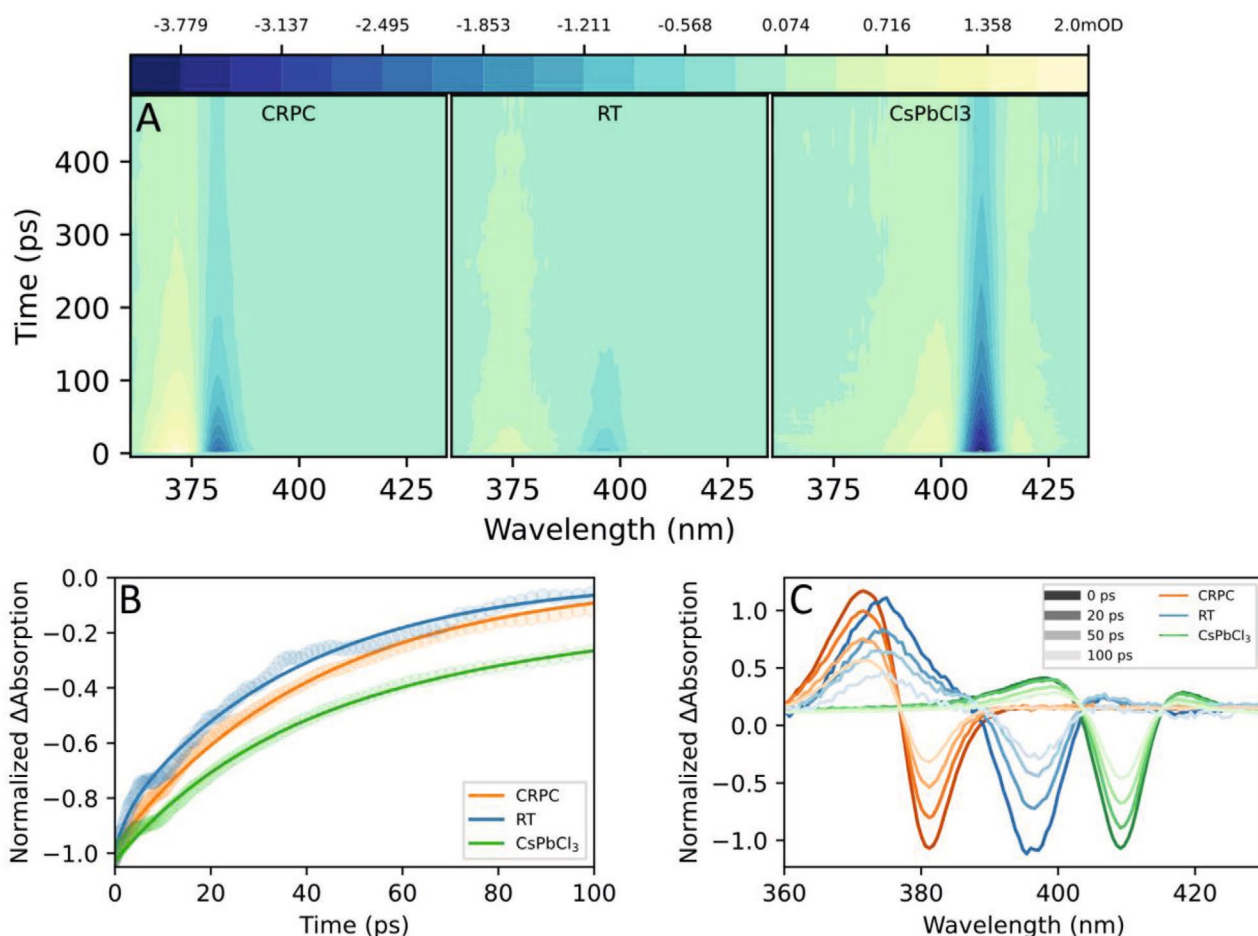

Figure 4. A) Transient absorption spectroscopy measurements of CRPC, RT, and $CsPbCl_3$ (from left to right) showing change in absorption spectra at increasing time delays in moD. B) Normalized change in absorption at the ground-state bleach over increasing time delay for CRPC (orange), RT (blue), and $CsPbCl_3$ (green). Data are plotted as circular markers while biexponential fits are plotted as solid lines. C) Transient absorption spectra from (A) at various time delays for CRPC (orange), RT (blue), and $CsPbCl_3$ (green).

However, RT decays more rapidly than CRPC. A biexponential fitting and normalization of the ground-state bleach data yielded a longer time constant of 81.7 ps for CRPC, compared to 69.7 ps for RT. The faster decay in RT can be attributed to trap-facilitated non-radiative recombination which in turn is a potential sign of phase segregation in RT.[19–21] Incomplete Rb-incorporation is known to cause traps, we posit that these traps are leading to the observed faster non-radiative recombination in RT.[4,22]

Figure 4c plots the bleach spectra at various delay times. The ground-state bleaches are consistent with the absorption spectra in Figure 3a. Notably, features for RT are broader compared to CRPC and $CsPbCl_3$. These broader features of RT are indicative of multiple phases in the material with slightly varying degrees of Rb incorporation. Halide phase segregation in perovskites exhibits a similar broadening of features.[21] Overall, TA yields multiple observations of higher trap density in RT than CRPC samples that can be attributed to incomplete Rb-incorporation, reinforcing that SPKT is required to thoroughly incorporate Rb into $CsPbCl_3$ without degrading the material with traps.

Through SPKT, the desired alloy becomes energetically favorable at high temperature.[8] Then by rapidly cooling the alloy, it becomes trapped and is sustained at room temperature. In contrast, gradual cooling of the alloy from high temperature allows heat dissipation and crystal reorientation.[7] Thus, if a kinetically trapped alloy is heated to high temperature and cooled gradually, the thermodynamically favored non-alloy phases are expected to re-emerge. Indeed, when we heat CRPC thin films to 250 °C and gradually cool to room-temperature, we find that the emission spectra progress towards those of $CsPbCl_3$ (Figure S5, Supporting Information). This suggests that there is a temperature <250 °C at which the CRPC has sufficient energy to transition out of its kinetically trapped state and into a more thermodynamically favorable state. With this final experiment, we conclude that our treatment indeed causes kinetic trapping in the material as this trapping can be reversed at sufficiently high temperatures.

3. Conclusion

This work demonstrates SPKT as a means to produce new halide perovskite alloys such as UV emitters. This stability of the perovskite is tested to ensure thorough alloying and TA observations reveal superior optical properties. The SPKT principle may, in the future, be extended to other spectral regimes of interest, such as the deeper UV and portions of the near-infrared.

4. Experimental Section

Materials and Chemicals: Cesium chloride (CsCl), lead chloride ($PbCl_2$), rubidium chloride (RbCl), and dimethyl sulfoxide (DMSO) were purchased from Sigma-Aldrich. Chloroform was purchased from DriSolv. All chemicals were used as received.

Solvent-Phase Kinetically Trapped CRPC Film Fabrication: The precursor solution was prepared by dissolving stoichiometric quantities of $PbCl_2$ (0.2 м, 55.6 mg), CsCl (0.04 м, 6.7 mg), and RbCl (0.16 м, 19.3 mg) in DMSO (1 mL) under continuous stirring for 2 h at 150 °C. Please see the work by Pina et al.[23] for details about substrate preparation and spin-coating. $CsPbCl_3$ films were synthesized with 0.05 м of CsCl and $PbCl_2$. Reversibility of the kinetically trapped CRPC was tested by synthesizing a film as outlined above and then annealing the film on the 250 °C hot plate for 10 min. Then, the hot plate was turned off and allowed to cool to 25 °C. Then, the film was characterized.

Structural Characterizations: X-ray diffractograms were recorded using a Rigaku MiniFlex 600 powder X-ray diffractometer equipped with a NaI scintillation counter and using monochromatized Cu Kα radiation (l = 0.15406 nm).

Optical Measurements: All UV–vis absorption was measured using a Perkin Elmer LAMBDA 950 UV/Vis/NIR spectrometer. For photoluminescence measurements, please see for the work by Pina et al.[23] for details.

Ultrafast Transient Absorption Spectroscopy: The pump source consisted of 330 nm wavelength femtosecond pulses (250 fs, FWHM) with a repetition rate of 5 kHz. The probe was a white-light continuum from (350–500 nm). These sources were generated from a regenerative amplified Yb:KGW laser (PHAROS, Light Conversion) with 1030 nm as the fundamental which was passed through a beam splitter. One arm of the beam was used to pump an optical parametric amplifier (ORPHEUS, Light Conversion) for the pump source and the other arm was focused into a CaF_2 crystal (Ultrafast Systems) to generate a UV–vis white-light continuum probe. Both arms were directed into a commercial transient absorption spectrometer (Helios, Ultrafast Systems). The probe pulse was delayed relative to the pump pulse to provide a time window of up to 7 ns.

First-Principle Calculations: Formation energies were obtained by performing first principle DFT calculations using the Vienna Ab Initio Simulation Package (VASP).[24] The crystal structure of orthorhombic $CsPbCl_3$ (mp-id mp-675524) was obtained from Materials Project.[25] Using Perdew–Burke–Ernzerhof (PBE) exchange-correlation functional with an energy cut-off of 500 eV and fermi level smearing of 0.1 eV, total energies of the systems were calculated on a k-points grid of size $4 \times 4 \times 4$ and centered at Gamma.[26] Structure optimization was performed till maximum force convergence less than 0.001 eV per atom was achieved. Formation energies were further calculated with respect to standard states of constituent elements which were then normalized to formation energy per atom. Pymatgen phase diagram was used to query Materials Project database to first benchmark the obtained formation energy results.[27] With consistent benchmarking settings, the formation energies were calculated for the rest of the compositions.

X-ray Photoelectron Spectroscopy (XPS): For XPS, thin films were prepared on indium tin oxide substrates instead of glass substrates. These samples were then mounted onto a stainless-steel plate and measurements were made using a Thermo Scientific K-Alpha system with an Al K alpha X-ray source; a take-off angle of 90° was used. The carbon 1s peak at 248.8 eV was used for calibration.

Supporting Information

Supporting Information is available from the Wiley Online Library or from the author.

Acknowledgements

Conflict of Interest

The authors declare no conflict of interest.

[1] B. R. Sutherland, E. H. Sargent, *Nat. Photonics* **2016**, *10*, 295.

[2] Y. Zhou, Z. Zhou, M. Chen, Y. Zong, J. Huang, S. Pang, N. P. Padture, *J. Mater. Chem. A* **2016**, *4*, 17623.

[3] Q. A. Akkerman, D. Meggiolaro, Z. Dang, F. De Angelis, L. Manna, *ACS Energy Lett.* **2017**, *2*, 2183.

[4] M. R. Linaburg, E. T. McClure, J. D. Majher, P. M. Woodward, *Chem. Mater.* **2017**, *29*, 3507.

[5] B. Tang, Y. Hu, H. Dong, L. Sun, B. Zhao, X. Jiang, L. Zhang, *Angew. Chem.* **2019**, *131*, 16280.

[6] C. C. Stoumpos, C. D. Malliakas, M. G. Kanatzidis, *Inorg. Chem.* **2013**, *52*, 9019.

[7] M. Lai, Q. Kong, C. G. Bischak, Y. Yu, L. Dou, S. W. Eaton, N. S. Ginsberg, P. Yang, *Nano Res.* **2017**, *10*, 1107.

[8] U.-G. Jong, C.-J. Yu, Y.-H. Kye, Y.-S. Kim, C.-H. Kim, S.-G. Ri, *J. Mater. Chem. A* **2018**, *6*, 17994.

[9] M. R. Filip, G. E. Eperon, H. J. Snaith, F. Giustino, *Nat. Commun.* **2014**, *5*, 5757.

[10] J. H. Lee, N. C. Bristowe, J. H. Lee, S. H. Lee, P. D. Bristowe, A. K. Cheetham, H. M. Jang, *Chem. Mater.* **2016**, *28*, 4259.

[11] R. G. Niemann, L. Gouda, J. Hu, S. Tirosh, R. Gottesman, P. J. Cameron, A. Zaban, *J. Mater. Chem. A* **2016**, *4*, 17819.

[12] D. Amgar, T. Binyamin, V. Uvarov, L. Etgar, *Nanoscale* **2018**, *10*, 6060.

[13] H. Y. Fan, *Phys. Rev.* **1951**, *82*, 900.

[14] M. Sebastian, J. A. Peters, C. C. Stoumpos, J. Im, S. S. Kostina, Z. Liu, M. G. Kanatzidis, A. J. Freeman, B. W. Wessels, *Phys. Rev. B: Condens. Matter Mater. Phys.* **2015**, *92*, 235210.

[15] Y. Yuan, J. Huang, *Acc. Chem. Res.* **2016**, *49*, 286.

[16] K. Wu, G. Liang, Q. Shang, Y. Ren, D. Kong, T. Lian, *J. Am. Chem. Soc.* **2015**, *137*, 12792.

[17] J. A. Christians, J. S. Manser, P. V. Kamat, *J. Phys. Chem. Lett.* **2015**, *6*, 2086.

[18] C. Luo, W. Li, D. Xiong, J. Fu, W. Yang, *Nanoscale* **2019**, *11*, 15206.

[19] A. Buin, R. Comin, J. Xu, A. H. Ip, E. H. Sargent, *Chem. Mater.* **2015**, *27*, 4405.

[20] R. Lai, K. Wu, *J. Chem. Phys.* **2019**, *151*, 194701.

[21] R. G. Balakrishna, S. M. Kobosko, P. V. Kamat, *ACS Energy Lett.* **2018**, *3*, 2267.

[22] H. Wang, X. Zhao, B. Zhang, Z. Xie, *J. Mater. Chem. C* **2019**, *7*, 5596.

[23] J. M. Pina, D. H. Parmar, G. Bappi, C. Zhou, H. Choubisa, M. Vafaie, A. M. Najarian, K. Bertens, L. K. Sagar, Y. Dong, Y. Gao, S. Hoogland, M. I. Saidaminov, E. H. Sargent, *Adv. Mater.* **2020**, *33*, 2006697.

[24] G. Kresse, J. Furthmüller, *Phys. Rev. B: Condens. Matter Mater. Phys.* **1996**, *54*, 11169.

[25] G. Ceder, K. P.-D. D. Explorer, http://www.osti.gov/dataexplorer (accessed: May 2020).

[26] M. Ernzerhof, G. E. Scuseria, *J. Chem. Phys.* **1999**, *110*, 5029.

[27] S. P. Ong, W. D. Richards, A. Jain, G. Hautier, M. Kocher, S. Cholia, D. Gunter, V. L. Chevrier, K. A. Persson, G. Ceder, *Comput. Mater. Sci.* **2013**, *68*, 314.